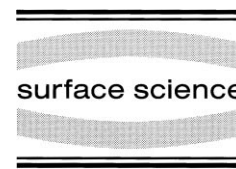




ELSEVIER

Surface Science 457 (2000) 219–228



www.elsevier.nl/locate/susc

Fourier transformed atomic force microscopy: tapping mode atomic force microscopy beyond the Hookian approximation

Robert W. Stark, Wolfgang M. Heckl *

Institut für Kristallographie und Angewandte Mineralogie, Universität München, Theresienstr. 41, 80333 Munich, Germany

Received 19 January 2000; accepted for publication 24 February 2000

Abstract

The periodic impact force induced by the tip–sample contact in tapping mode atomic force microscopy (TM-AFM) gives rise to anharmonic oscillations of the sensing cantilever. These anharmonic signals can be understood with a model which goes beyond the common Hookian approximation: the cantilever is described as a multiple degree of freedom system. A theoretical analysis of the anharmonic signals in the light of the extended model shows that these signals contain information on the elastic properties of the specimen surface. In Fourier transformed operation mode of TM-AFM the anharmonic oscillations are analyzed in the frequency domain. This allows for the reconstruction of characteristics of the tip–sample force, like contact time and maximum contact force. © 2000 Elsevier Science B.V. All rights reserved.

Keywords: Atomic force microscopy; Computer simulations

1. Introduction

For the investigation of elastic properties of surfaces of hard specimens, like semiconductors, alloys or ceramics, dynamic contact mode force microscopy has become a valuable tool. In the ultrasonic or acoustic imaging mode, ultrasonic waves are coupled either directly to the scanning cantilever or to the specimen, while the tip is in direct contact with the specimen. Investigation of the cantilever response in the frequency domain allows us to determine mechanical characteristics of the tip–sample contact: stiffness by ultrasonic/acoustic microscopy [1–3], friction by acoustic friction microscopy [4,5], and lateral

stiffness by torsional overtone microscopy [6]. In order to understand the frequency response in these contact imaging modes, the cantilever must be described as a multiple degree of freedom system in order to reproduce the higher degree resonances of the system.

In intermittent contact microscopy, basically two operational modes can be distinguished. If the cantilever is driven well below the fundamental resonance frequency, surface forces can be acquired quasi-statically in pulsed force mode [7]. In contrast, if the cantilever is driven near to or at its resonant frequency, like in tapping mode atomic force microscopy (TM-AFM) [8], a dynamic model has to be applied. A one degree of freedom approximation for the cantilever is widely used in order to describe TM-AFM. There, the cantilever is described as a Hookian spring, where a lumped mass is attached. The mass interacts

* Corresponding author. Fax: +49-89-23944331.
E-mail addresses: robert@nanomanipulation.de
(R.W. Stark), w.heckl@lrz.uni-muenchen.de (W.M. Heckl)

periodically with the surface, which allows us to describe the system by a grazing impact harmonic oscillator model [9]. It was shown that experimental data and theory using harmonic approximation agree sufficiently well [10,11]. However, anharmonic signal components could be observed experimentally in TM-AFM when the setpoint was adjusted in a way which is referred to as ‘hard tapping’ [12]. In several recent studies, dynamic behavior of the tapping cantilever was reported experimentally [13,14] and theoretically [15], which is inconsistent with a simple harmonic approximation.

Anharmonic cantilever dynamics can be attributed to non-linear interactions induced by the tip–sample contact, or in the surrounding viscous media. For dynamic contact mode microscopy the response of a surface coupled cantilever was investigated theoretically [16] and experimentally [17]. For intermittent contact force microscopy a similar approach is feasible. This means that the cantilever has to be described within a framework of a multiple degree of freedom system with harmonic (driving) and anharmonic (tip–sample interaction) external forces.

Very recently, it was shown experimentally that the periodic impact of the tip on the sample in tapping mode atomic force microscopy induces high-frequency ultrasonic vibrations of the cantilever [18,19]. Harmonics of the working (driving) frequency of about 45 kHz were prominent in the photodiode signal. The harmonic distortion of the photodiode signal was much larger than would be expected from the inherent harmonic distortion of the excitation. The main source of the harmonic distortion is the non-linearity of the tip–sample interaction. In a first and simple approach the periodic mechanical tip–sample interaction can be understood as an arbitrary periodic external force, which acts on the free end of the cantilever. This periodic, but anharmonic, force introduces higher frequency components into the system.

In this article, we discuss a simple semi-analytical approach, where the multiple degree of freedom dynamics of a cantilever in tapping mode are investigated with respect to elastic surface properties.

2. Theory

2.1. General

For the application of the theory of small cantilever deflections, several conditions have to be fulfilled. (i) The oscillation amplitudes must be very small compared with the dimensions of the cantilever. In TM-AFM the amplitudes range typically from 1 to 100 nm. In contrast, a typical cantilever has a thickness of 500 nm or more. Therefore, a theory of small deflections is appropriate. (ii) The cantilever material can be described as a linear and homogeneous continuum. This is usually fulfilled for microfabricated cantilevers. (iii) The wavelength of the cantilever oscillations must be smaller than the beam thickness. This was shown to be valid for the first 30 eigenmodes [20]. As will be shown in the following, few eigenmodes are needed to model the cantilever dynamics.

The one-dimensional Euler–Bernoulli equation governs the dynamics of a rectangular cantilever. For the model calculations here, let the mass density of the material $m(x)$, the moment of inertia $I(x)$, and Young’s modulus $E(x)$ be constant. The mass of the tip is neglected. Thus, the equation of motion for transversal cantilever vibrations is

$$EI \frac{\partial^4}{\partial x^4} \left[w(x,t) + a_1 \frac{\partial w(x,t)}{\partial t} \right] + m(x) \frac{\partial^2 w(x,t)}{\partial t^2} + a_0 m(x) \frac{\partial w(x,t)}{\partial t} = f(x,t). \quad (1)$$

Here, $w(x,t)$ is the time-dependent transverse displacement of the centerline from the neutral position. Damping is modeled by two parameters: the parameter a_0 describes the mass proportional damping, whereas a_1 is a stiffness proportional damping parameter. (For a comparative study on theory and experiment of cantilever eigenmodes, cf. Ref. [17].)

Fig. 1 illustrates the different forces in TM-AFM. The cantilever is driven by harmonic displacements of the base, whereas anharmonic forces are introduced by the tapping tip. The first step in order to investigate the cantilever, which is periodically excited by an external force, is to transform Eq. (1) into a suitable set of normal

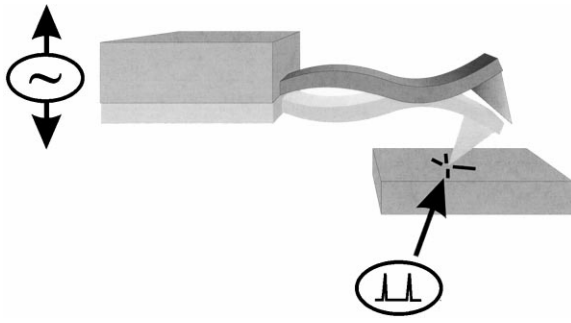


Fig. 1. Principle of tapping mode AFM. The cantilever is excited harmonically at the base. The periodic impact of the tip on the sample gives rise to anharmonic contributions in the signal.

coordinates. This yields a set of decoupled harmonic oscillators. Then, the arbitrary external load is expressed in a Fourier series, which subsequently allows us to calculate the response of each individual harmonic oscillator. Finally, the total geometric response of the cantilever beam is obtained by summation of the individual harmonic oscillators.

2.2. Response to an arbitrary periodic external load

The eigenfunctions $\varphi_n(x)$ of the undamped system [Eq. (A.7)] constitute a useful coordinate system for the description of the freely vibrating cantilever under an external load. Applying the transformation rule

$$w(x,t) = \sum_{n=1}^{\infty} \varphi_n(x) Y_n(t) \quad (2)$$

Eq. (1) can be transformed into a set of decoupled ordinary differential equations

$$\ddot{Y}_i(t) + 2\gamma_i\omega_i \dot{Y}_i(t) + \omega_i^2 Y_i(t) = \frac{F_i(t)}{M_i}, \quad i=1, 2, \dots \quad (3)$$

(see Appendix B). The generalized force F_i , generalized mass M_i , and damping parameter γ_i are discussed in Appendix B. For harmonic forces $F_i(t)$ the stationary amplitudes for the respective eigenmodes φ_i as derived from Eq. (3) are

$$Y_i(t) = \frac{F_i}{K_i} \frac{(1 - \beta_i^2) - i(2\gamma_i\beta_i)}{(1 - \beta_i^2)^2 + (2\gamma_i\beta_i)^2} \exp(i\Omega t) \quad (4)$$

with $\beta_i = \Omega/\omega_i$ as the frequency ratio between driving force and the respective resonant frequency ω_i . The generalized stiffness is $K_i = M_i\omega_i^2$.

Now, the response of the cantilever to an arbitrary external loading has to be derived. A periodic but arbitrarily shaped generalized excitation function $F_i(t)$ with base frequency Ω can be expanded in a Fourier series (with complex coefficients $c_{i,k}$)

$$F_i(t) = \sum_{k=-\infty}^{\infty} c_{i,k} \exp(ik\Omega t). \quad (5)$$

Thus, the time-dependent stationary amplitude response of the individual modes φ_i is given by

$$Y_i(t) = \frac{1}{K_i} \sum_{k=-\infty}^{\infty} \frac{(1 - \beta_{i,k}^2) - i(2\gamma_i\beta_{i,k})}{(1 - \beta_{i,k}^2)^2 + (2\gamma_i\beta_{i,k})^2} c_{i,k} \times \exp(ik\Omega t). \quad (6)$$

Also here, the frequency ratio is $\beta_{i,k} = k\Omega/\omega_i$. Introducing the complex coefficients

$$c_{i,k}^Y = \frac{1}{K_i} \frac{(1 - \beta_{i,k}^2) - i(2\gamma_i\beta_{i,k})}{(1 - \beta_{i,k}^2)^2 + (2\gamma_i\beta_{i,k})^2} c_{i,k} \quad (7)$$

the steady state response to an arbitrary but periodic external force can be written conveniently

$$w(x,t) = \sum_{i=1}^{\infty} \varphi_i(x) \sum_{k=-\infty}^{\infty} c_{i,k}^Y \exp(ik\Omega t). \quad (8)$$

Usually, in an AFM the derivative at the end of the cantilever at $x=L$ is measured by a light-lever set-up. Thus, the photodiode signal is

$$S(t) = \sum_{i=1}^{\infty} \varphi_i'(L) \sum_{k=-\infty}^{\infty} c_{i,k}^Y \exp(ik\Omega t). \quad (9)$$

Note that throughout this paper Eq. (9) is employed in order to calculate the photodiode signal. The numerical value is given in nanometers, which is a nominal value as it would be obtained using a quasi-statically calibrated light-lever detection AFM. In Ref. [20] this nominal value is referred to as ‘virtual deflection’. In order to calculate the true tip deflection, Eq. (8) must be used instead of Eq. (9).

2.3. Tip-sample force

The periodic force induced by the impact is now integrated into the model. In order to avoid complicated numerical simulations of the grazing impact cantilever, a first order approximation is made: the tip-sample force is calculated from a numerical model employing only a one degree of freedom approximation, higher order cantilever resonances are neglected. From this numerical model, the tip-sample force is extracted and used as a parameter in the more complex multiple degree of freedom system derived in the previous section.

In order to allow the first order approximation of the tapping forces $f^{\text{tap}}(x,t)$, the boundary conditions for a freely oscillating cantilever have to be fulfilled for most of the cycle time. In other words: (iv) the higher degree oscillation amplitudes A_k ($k > 1$) are small compared with the fundamental oscillation A_1 ($A_k \ll A_1$); (v) the tip sample contact time $t' = \tau T$ is short compared with the cycle T .

The differential equation for a single degree of freedom tapping cantilever in the framework of Hertzian contact mechanics is then given by

$$\ddot{y} + 2\gamma\omega_0\dot{y} + \omega_0^2[y - y^s - A^d \sin(\Omega t)] = \begin{cases} 0 & \text{if } y < -A^s \\ f(y) & \text{else} \end{cases} \quad (10)$$

with

$$f(y) = \frac{\omega_0^2}{k} \kappa_{\text{eff}} R^{1/2} d^{3/2}(y) \quad (11)$$

where ω_0 is the resonant frequency and γ the damping coefficient (cf. Ref. [9], for other models of contact mechanics applied to TM-AFM cf. e.g. Ref. [21] or Ref. [22]). For the sake of simplicity, only repulsive contact mechanics are assumed, attractive forces are neglected. R is the radius of the AFM tip, y^s the distance between the zero position of the tip and the sample, A^d the driving amplitude at the cantilever base, and $d[y(t)] = y(t) - y^s$ if $y < 0$ is the indentation of the tip into the sample. The parameter which describes the elastic properties of the sample (and the tip) is

the effective stiffness

$$\kappa_{\text{eff}} = \frac{4}{3\pi^2} \left[\frac{1 - \nu_1^2}{E_1} + \frac{1 - \nu_2^2}{E_2} \right]^{-1} \quad (12)$$

with the respective Young's moduli E_i and Poisson ratio ν_i . By numerical solution of Eq. (11) the periodic anharmonic interaction force is determined. For an analytical description of the multiple degree of freedom system, the Fourier series for the tip-sample force $f^{\text{tap}}(x,t)$ has to be derived. The impact force acts only on the free end of the cantilever at $x=L$, thus

$$f^{\text{tap}}(x,t) = \delta(x-L)g^{\text{tap}}(t). \quad (13)$$

The function $g^{\text{tap}}(t)$ is the time-dependent interaction force as derived from the numerical simulation, $\delta(x)$ is the Dirac delta function.

The generalized total force $F_i(t)$ acting on the cantilever has two constituents: the periodic but anharmonic generalized impact $F_i^{\text{tap}}(t)$, and the external driving force $F_i^{\text{drive}}(t)$:

$$F_i(t) = F_i^{\text{tap}}(t) + F_i^{\text{drive}}(t) = \int_0^L f^{\text{tap}}(x,t)\varphi_i(x)dx + \int_0^L f^{\text{drive}}(x,t)\varphi_i(x)dx. \quad (14)$$

However, for the investigation of higher degree harmonic terms, only F_i^{tap} has to be discussed in detail, because F_i^{drive} is harmonic. The generalized interaction force is derived from Eq. (13). Integration yields

$$F_i^{\text{tap}}(t) = \varphi_i(L)g^{\text{tap}}(t). \quad (15)$$

The function $g^{\text{tap}}(t)$ is a convolution of the impact function for a single impact $h(t)$ with a Dirac comb

$$g^{\text{tap}}(t) = h(t) * \sum_{k=-\infty}^{\infty} \delta\left(t - \Delta\vartheta - k \frac{2\pi}{\Omega}\right). \quad (16)$$

The relative time delay with respect to the cycle duration of the pulses is $\Delta\vartheta$. Using the Parseval theorem, the Fourier expansion $S_{g(t)}$ of the impact function $g^{\text{tap}}(t)$ is obtained

$$S_{g(t)} = \sum_{k=-\infty}^{\infty} c_k \exp(ik\Omega t) = \sum_{k=-\infty}^{\infty} c_k^h c_k^\delta \exp(ik\Omega t). \quad (17)$$

The complex Fourier coefficients of $h(t)$ and the Dirac comb are

$$c_k^h = \frac{1}{T} \int_0^T h(t) \exp(-ik\Omega t) dt \quad (18)$$

$$c_k^\delta = \frac{1}{2} [\sin(k\Omega\Delta\vartheta) - i \cos(k\Omega\Delta\vartheta)]. \quad (19)$$

The amplitude coefficients $A_k^\delta = 2\|c_k^\delta\| = 1$ are constant. This means that the c_k^δ determine the phase relation, but not the amplitude of the signal. Therefore, a discussion of the amplitudes of the individual harmonic terms can be limited to the coefficients c_k^h .

3. Results and discussion

In the following, the detection of higher harmonic signals as image information is investigated within the framework of the theory. As a numerical example, the material parameters of a silicon wafer surface are used.

The cantilever parameters used in the calculations are: resonant frequency of the fundamental mode $f_1 = 100$ kHz, spring constant $c = 20$ N/m, quality factors $Q_1 = 100$, $Q_2 = 417$, $Q_3 = 340$, $Q_4 = 200$, $Q_5 = 26$, i.e. $\gamma_1 = 0.005$, $\gamma_2 = 0.0012$, $\gamma_3 = 0.0015$, $\gamma_4 = 0.0025$, $\gamma_5 = 0.019$, and tip radius $R = 10$ nm. The sample parameters correspond to a silicon (100) surface with a Young's modulus of $E_{\langle 100 \rangle} = 129$ GPa. Attractive surface forces are neglected. The amplitude of the freely vibrating tip is $A^{\text{tip}} = 30$ nm, and the average distance between the zero position of the cantilever and the specimen surface is $A^{\text{set}} = 20$ nm. The distance between the zero deflection of the cantilever and the sample surface is kept constant. On hard

specimens, like the silicon surface here, this represents a standard tapping mode AFM with amplitude feedback. In order to determine the sensitivity of the cantilever signals to changes in the surface elasticity, additional calculations were carried out for an inhomogeneity, which is 10% softer with $E_{\text{inh}} = 116.1$ GPa (i.e. 90% $E_{\langle 100 \rangle}$). The effective contact stiffness of the tip-sample contact κ_{eff} [Eq. (12)] is the key parameter for the dynamics of the anharmonic contributions. Due to the choice of the numerical material parameters, κ_{eff} varies by 5.5%. The material parameters and the results of the numerical solution of Eq. (10) are summarized in Table 1.

In the next step, the solution of Eq. (10) is used to determine the parameterization of the tip-sample contact as external force. The impact $g^{\text{tap}}(t)$ as derived from the numerical simulation is shown in Fig. 2. In order to simplify further calculations, the numerical solution is approximated by

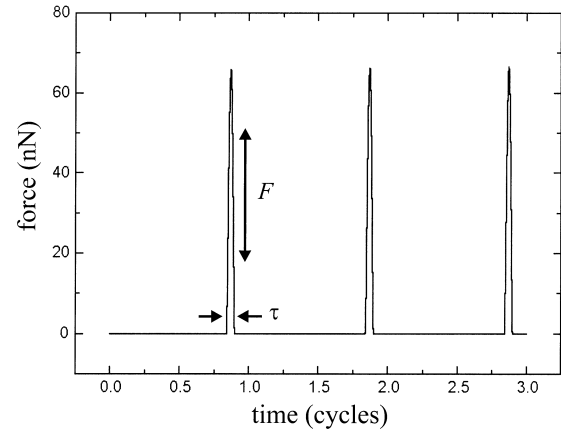


Fig. 2. The periodic impact force as determined by the numerical simulation for the one degree of freedom system. The relative contact time τ and the contact force F are defined as indicated.

Table 1

Parameters used for the numerical simulation: Young's modulus E and Poisson ratio ν . The values are valid for a silicon (100) wafer surface and a 10% softer inhomogeneity (Inh). Numerical results are the maximum indentation d of the tip into the sample, the maximum force F , the maximum stress P , the phase angle between free and tapping oscillation θ , and the relative contact time τ

Material	E (GPa)	ν	d (nm)	F (nN)	P (GPa)	θ ($^\circ$)	τ
Si	129.0	0.28	0.56	66.1	8.6	-47.19	0.0518
Inh	116.1	0.28	0.57	65.1	8.2	-47.23	0.0526

an empirical function which is determined by both of the most important parameters: the contact time $t' = \tau T$ and the maximum contact force F . A cut cosine function is a good approximation for the numerical values and provides a simple analytical Fourier expansion. The empirical approximation $h(t)$ for a single cycle is

$$h(t) = F \cos\left(\frac{\pi}{\tau T} t\right) \left[\theta\left(t - \frac{\tau T}{2}\right) - \theta\left(t - \frac{\tau T}{2}\right) \right] \quad (20)$$

with $\theta(t)$ as the step function. Substituting Eq. (20) into Eq. (18) yields the coefficients

$$c_k^h = \frac{2F\tau}{\pi} \frac{\cos(\tau k \pi)}{1 - 4\tau^2 k^2}. \quad (21)$$

For this special choice of the impact function $h(t)$ is symmetric, i.e. $h(t) = h(-t)$, thus $\text{Im } c_k^h = 0$. The coefficients are plotted in Fig. 3a. Note that the Fourier coefficients could also have been determined by fast Fourier transformation (FFT) from the numerical results. However, the empirical function allows us to verify the results analytically.

The photodiode signal response can be calculated by substituting the Fourier coefficients of Eq. (21) into Eq. (9) and using the cantilever parameters. In Fig. 3a the photodiode signal is depicted in the frequency domain. The dominant component for the cantilever dynamics is at the fundamental frequency. The self-consistency of the model can be checked by phase correct addition of the oscillatory motion caused by the component at the fundamental frequency to the free oscillatory motion of the cantilever. As a result, one obtains a good approximation for the single degree of freedom cantilever dynamics as obtained by the numerical solution of Eq. (10).

The other prominent frequency is the sixth harmonic. Here, the theoretical signal amplitude is equivalent to a static deflection of 0.19 nm. The relative contrast $c_{\text{rel}} = 1 - S_{\text{Si}}/S_{\text{Inh}}$ between the signal expected on pure silicon S_{Si} and the signal on the 10% softer sample S_{Inh} is 0.3%. However, as can be seen in Fig. 3b, the relative contrast increases with increasing frequency. For imaging purposes, the harmonics 17 and 18 are well suited.

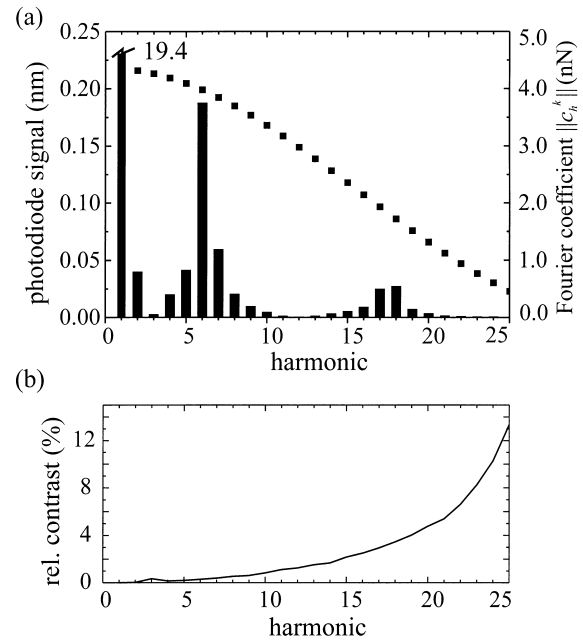


Fig. 3. (a) Photodiode signal of the tapping cantilever in the frequency domain [bars, cf. Eq. (9)]. The bar indicating the amplitude of the fundamental frequency was shortened in order to fit into the graphics. The multiple resonances of the cantilever beam are evident. The squares indicate the respective Fourier coefficients of the impact function in Eq. (17). (b) Relative contrast between both the silicon and the softer area. For the higher harmonics the contrast increases significantly.

The signal amplitude is still about 0.025 nm and the relative image contrast is now $c_{\text{rel}} = 3\%$. In phase imaging mode, a phase shift of 0.03° is obtained, cf. Table 1. Therefore, the low-level signals require a highly sensitive low-noise experimental set-up.

In the time domain, the photodiode signal exhibits complex behavior (Fig. 4). In the unfiltered photodiode signal (Fig. 4, top) only small deviations from the harmonic response can be determined. However, when the contributions of the fundamental frequency are removed from the signal, the high frequency oscillations become prominent (Fig. 4, bottom). The amplitudes of these anharmonic oscillations are two orders of magnitude smaller compared with the fundamental oscillation. This again justifies the approach to parameterize the tip-sample force as an external force.

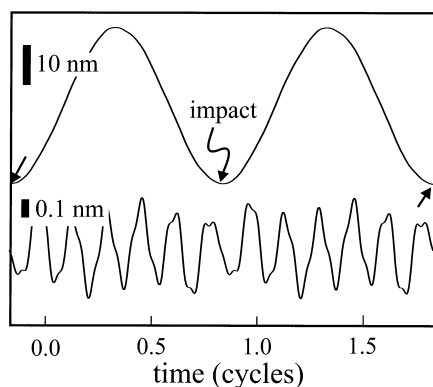


Fig. 4. Photodiode signal of the tapping cantilever in the time domain. In the unfiltered signals small distortions can be seen (top). The periodic tip-sample impact is indicated by the arrows. When the fundamental oscillation is filtered out, complex dynamics are evident (bottom).

The simplifying assumptions impose some limitations which should be reviewed briefly. The tip-sample force was chosen as an external force. This means that the cantilever is treated as a freely vibrating cantilever. Obviously, this assumption does not hold for the time when the cantilever is in contact with the specimen. Thus, for configurations like tapping on soft polymers, where the contact time is a significant fraction of the oscillation cycle, a fully numerical approach seems feasible.

In Eq. (6) a periodic external force was assumed, i.e. the system is treated as a linear system. This is not fulfilled for low setpoints (hard tapping) where non-linear effects can play a significant role in the cantilever dynamics. The same applies to the chaotic regime of the cantilever dynamics, where period doubling can occur [23] and additional spectral components can be introduced [24].

Another factor is that the resonant frequencies of the higher eigenmodes depend on the tip-sample interaction. However, for a semi-empirical approach this is not a real limitation. Similar to experiments, where the frequency shift of the oscillating cantilever was determined for conventional TM or non-contact AFM [25–27], the frequency vs. setpoint relation can be determined for the higher eigenmodes. The values obtained there can

subsequently be used for a semi-empirical formulation.

Finally, we would like to point out that the analysis of the cantilever dynamics in the frequency domain allows us to determine features of the tip-sample interaction. In a first approach, both key parameters of the tip-sample interaction can be determined: contact time τ and maximum loading force F . Basically, only the amplitudes of two higher harmonics have to be determined with sufficient accuracy. Together with the knowledge of the cantilever resonance frequencies and the corresponding quality factors, which can easily be measured, the parameters τ and F in Eq. (20) can be calculated. In a more sophisticated approach, all accessible Fourier components are used in order to reconstruct the tip-sample force by inverse Fourier transformation. Then, details of the impact, like attractive forces, can also potentially be analyzed.

In other words, with Fourier transformed AFM (FT-AFM) additional information on the tip-sample interaction is acquired. Phase imaging has opened the possibility to monitor energy dissipation in TM-AFM. With FT-AFM contact time τ and force F , i.e. elastic properties, can also be addressed.

4. Conclusions

In summary, we have shown theoretically that the dynamics of tapping mode AFM are anharmonic. For a beam shaped cantilever, anharmonic oscillations with order of magnitude 1% of the harmonic oscillation can be expected. Furthermore, we have shown that the anharmonic signal components can be used to obtain an image contrast on hard samples based on the differences in contact stiffness. With a silicon (100) surface as numerical example, we show that elastic inhomogeneities having a 10% lower Young's modulus yield a significant contrast in higher harmonics.

The main advantage of the discussed imaging mode is that the interaction force itself can be measured. This significantly enhances the number of possible applications for dynamic intermittent contact mode atomic force microscopy. Dissipative

effects can be addressed using phase imaging AFM, whereas the elastic tip-sample interaction can be investigated by Fourier transformed AFM.

Acknowledgements

We thank R. Hillenbrand, M. Stark, R. Guckenberger, F. Keilmann (all MPI für Biochemie, Martinsried, Germany) and T. Drobek for fruitful discussions. This work was supported by Grant BMBF 13N7509.

Appendix A: The freely oscillating cantilever

The solution of the equation of motion of a freely vibrating cantilever can be found in textbooks on structural dynamics [28,29]. Therefore, the solution is only briefly reviewed here in order to provide the necessary equations. The undamped free vibration equation of motion for the transverse displacement response $w(x,t)$ of a cantilever beam is

$$EI \frac{\partial^4 w(x,t)}{\partial x^4} + m \frac{\partial^2 w(x,t)}{\partial t^2} = 0 \quad (\text{A.1})$$

with flexural stiffness EI and constant mass per unit length m . The variables can easily be separated using

$$w(x,t) = \varphi(x)Y(t). \quad (\text{A.2})$$

Here, $\varphi(x)$ is the specific shape and $Y(t)$ the time-dependent amplitude. Substitution of Eq. (A.2) into Eq. (A.1) and division by $\varphi(x)Y(t)$ allows us to obtain the separated ordinary differential equations

$$\ddot{Y}(t) + \omega^2 Y(t) = 0 \quad (\text{A.3})$$

$$\frac{d^4}{dx^4} \varphi(x) + \frac{\omega^2 m}{EI} \varphi(x) = 0 \quad (\text{A.4})$$

where the constant ω can be found (see below) to fulfil the relation

$$\omega_n^2 = (k_n L)^4 \frac{EI}{m}. \quad (\text{A.5})$$

Eq. (A.3) is the well-known undamped one degree of freedom harmonic oscillator. The modal shapes can be derived from Eq. (A.4) when the boundary conditions are considered. On the left-hand side at $x=0$ the boundary conditions are $\varphi(0)=0$ and $\varphi'(0)=0$, which is a clamped end. On the free end of the cantilever at $x=L$, the corresponding equations are $\varphi''(L)=0$ and $\varphi'''(L)=0$.

In the following, the solutions obtained from Eq. (A.4) are given without derivation. The eigenvalues [Eq. (A.5)] are determined by the characteristic (frequency) equation

$$1 + \cos k_n L \cosh k_n L = 0. \quad (\text{A.6})$$

Numerical values are: $k_1 L = 1.875$, $k_2 L = 4.694$, and $k_3 L = 7.854$. For higher eigenmodes the asymptotic value is $k_n^{(a)} L = (n - \frac{1}{2})\pi$, a good approximation. Already for $n=4$ the asymptotic value provides a four-place accuracy approximation for the exact solution.

The eigenvectors (modal shapes) for the freely vibrating cantilever are

$$\begin{aligned} \varphi_n(x) = & \cos k_n x - \cosh k_n x - \frac{\cos k_n L + \cosh k_n L}{\sin k_n L + \sinh k_n L} \\ & \times (\sin k_n x - \sinh k_n x). \end{aligned} \quad (\text{A.7})$$

The $\varphi_n(x)$ fulfil the orthogonality relation

$$\int_0^L \varphi_n(x) \varphi_m(x) dx = 0 \quad \text{for } \omega_n \neq \omega_m. \quad (\text{A.8})$$

Furthermore, the $\varphi_n(x)$ are normalized

$$\int_0^L \varphi_n(x) \varphi_n(x) dx = 1. \quad (\text{A.9})$$

At $x=0$ and $x=L$ Eq. (A.7) yields

$$\varphi_n(0) = 0 \quad (\text{A.10})$$

$$\varphi_n(L) = 2(-1)^n. \quad (\text{A.11})$$

From a geometric point of view, the eigenvectors are the modal bending shapes $\varphi_n(x)$. They can be used as normal coordinates for the description of a general cantilever motion. Note that the $\varphi_n(x)$ constitute an incomplete baseset. However, they

span the subspace of the physically possible bending shapes of a freely oscillating cantilever.

Appendix B: Transformation into generalized coordinates

For the description of the cantilever dynamics the eigenfunctions of the respective configuration are used as coordinate system. The transformation rule into the normal coordinates is given by

$$w(x,t) = \sum_{n=1}^{\infty} \varphi_n(x) Y_n(t) \tag{B.1}$$

where the $\varphi_n(x)$ are the modal shapes and the $Y_n(t)$ the respective time-dependent amplitudes. In the following, the $\varphi_n(x)$ are assumed to be orthonormal, but no further assumptions concerning the shape are needed. Therefore, the conclusions drawn in this appendix apply to arbitrary boundary conditions.

Substitution of Eq. (B.1) into Eq. (1) yields

$$\begin{aligned} \sum_{n=1}^{\infty} EI \frac{\partial^4}{\partial x^4} [\varphi_n(x) Y_n(t) + a_1 \varphi_n(x) \dot{Y}_n(t)] \\ + \sum_{n=1}^{\infty} m \varphi_n(x) \ddot{Y}_n(t) + \sum_{n=1}^{\infty} a_0 \varphi_n(x) \dot{Y}_n(t) = f(x,t). \end{aligned} \tag{B.2}$$

Multiplication by $\varphi_n(x)$, integration and subsequent application of the orthogonality relation [Eq. (A.8)] give

$$\begin{aligned} M_i \ddot{Y}_i(t) + \sum_{n=1}^{\infty} \dot{Y}_i(t) \int_0^L \varphi_n(x) \\ \times \left[a_0 \varphi_n(x) + a_1 EI \frac{\partial^4 \varphi_n(x)}{\partial x^4} \right] dx \\ + \omega_i^2 M_i Y_i(t) = F_i(t). \end{aligned} \tag{B.3}$$

The generalized mass M_i is defined by

$$M_i = \int_0^L m(x) \varphi_i(x)^2 dx. \tag{B.4}$$

Here, $M_i = m$ because the $\varphi_i(x)$ are normalized and m is independent of x . In order not to restrict the

results unnecessarily, throughout this article the generalized mass M_i will be used. Similarly, the generalized external force is

$$F_i(t) = \int_0^L f(x,t) \varphi_i(x) dx \tag{B.5}$$

and the generalized stiffness is

$$K_i = \int_0^L \varphi_i(x) \frac{\partial^2}{\partial x^2} EI(x) \frac{\partial^2}{\partial x^2} \varphi_i(x) dx. \tag{B.6}$$

The damping terms in Eq. (1) were chosen so that Eq. (B.3) decouples completely. The modal damping parameter γ_i is thus given by

$$\gamma_i = \frac{a_0}{2\omega_i} + \frac{a_1 \omega_i}{2}. \tag{B.7}$$

This means that the parameter γ can arbitrarily be selected for two eigenfrequencies ω_n and ω_m in order to reproduce experimental values. (Often the quality factor $Q_i = 1/2\gamma_i$ is used instead of the damping coefficients γ_i .) By this choice all other damping parameters are determined. The experimental values are qualitatively well reproduced using this approach. For low frequencies, the damping is reduced with increasing eigenfrequency, for higher eigenfrequencies the damping increases linearly (Fig. B.1).

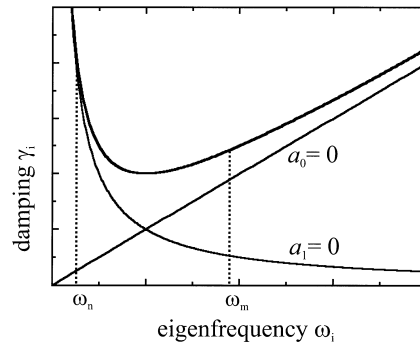


Fig. B.1. Damping for the different eigenmodes. For small eigenfrequencies stiffness proportional damping dominates, whereas for larger frequencies the mass dependent damping prevails [see Eq. (1)].

This now allows further transformation of Eq. (B.3) and leads to the decoupled differential equations

$$\ddot{Y}_i(t) + 2\gamma_i\omega_i \dot{Y}_i(t) + \omega_i^2 Y_i(t) = \frac{F_i(t)}{M_i} \quad i = 1, 2, \dots \quad (\text{B.8})$$

References

- [1] K. Yamanaka, H. Ogiso, O. Kolosov, Appl. Phys. Lett. 64 (1994) 178.
- [2] U. Rabe, W. Arnold, Appl. Phys. Lett. 64 (1994) 1493.
- [3] O. Kolosov, M. Castell, C. Marsh, A. Brix, Phys. Rev. Lett. 81 (1998) 1046.
- [4] K. Wahl, S. Stepnovski, W. Unertl, Tribol. Lett. 5 (1998) 103.
- [5] V. Scherer, W. Arnold, B. Bhushan, Surf. Interface Anal. 27 (1999) 578.
- [6] T. Drobek, R. Stark, M. Gräber, W. Heckl, New J. Phys. 1 (1999) 15.1.
- [7] T. Miyatani, M. Horii, A. Rosa, M. Fujihira, O. Marti, Appl. Phys. Lett. 71 (1997) 2632.
- [8] Q. Zhong, D. Inniss, K. Kjoller, V. Elings, Surf. Sci. 290 (1993) L688.
- [9] J. Hunt, D. Sarid, Appl. Phys. Lett. 72 (1998) 2969.
- [10] G. Bar, R. Brandsch, M.-H. Whangbo, Surf. Sci. 411 (1998) L802.
- [11] M.-H. Whangbo, G. Bar, R. Brandsch, Surf. Sci. 411 (1998) L794.
- [12] J. Cleveland, B. Anczykowski, A. Schmid, V. Elings, Appl. Phys. Lett. 72 (1998) 2613.
- [13] R. Stark, T. Drobek, W. Heckl, Appl. Phys. Lett. 74 (1999) 3296.
- [14] S. van Noort, O. Willemsen, K. van der Werf, B. de Groot, J. Greve, Langmuir 15 (1999) 7101.
- [15] J. Tamayo, Appl. Phys. Lett. 75 (1999) 3569.
- [16] S. Hirsekorn, U. Rabe, W. Arnold, Nanotechnology 8 (1997) 57.
- [17] U. Rabe, K. Janser, W. Arnold, Rev. Sci. Instrum. 67 (1996) 3281.
- [18] R. Stark, W. Heckl, in preparation.
- [19] R. Hillenbrand, M. Stark, R. Guckenberger, Appl. Phys. Lett., in press.
- [20] H. Butt, M. Jaschke, Nanotechnology 6 (1995) 1.
- [21] B. Anczykowski, D. Krüger, H. Fuchs, Phys. Rev. B 53 (1996) 15485.
- [22] N. Burnham et al., Nanotechnology 8 (1997) 67.
- [23] N. Sasaki et al., Appl. Phys. A 66 (1998) S287.
- [24] N. Burnham, A. Kulik, G. Gremaud, G. Briggs, Phys. Rev. Lett. 74 (1995) 5092.
- [25] F. Giessibl, Phys. Rev. B 56 (1998) 16010.
- [26] U. Dürig, Appl. Phys. Lett. 75 (1999) 433.
- [27] S. He, T. Uda, K. Terakura, Phys. Rev. B 59 (1999) 13267.
- [28] R. Clough, J. Penzien, Dynamics of Structures, second ed., McGraw-Hill, Singapore, 1993.
- [29] M. Géradin, D. Rixen, Mechanical Vibrations: Theory and Application to Structural Dynamics, second ed., Wiley, New York, 1997.